

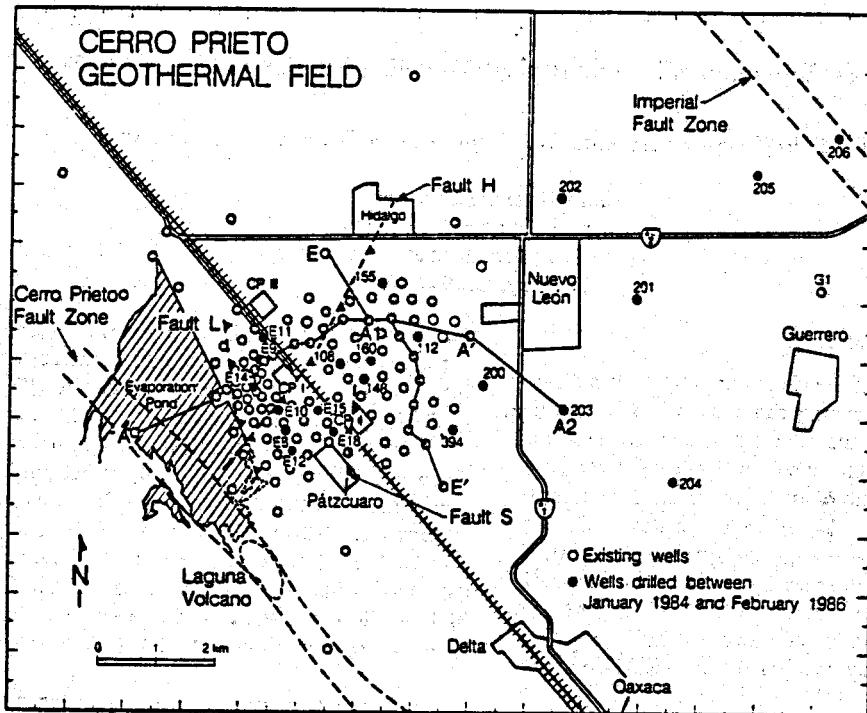
NOTICE CONCERNING COPYRIGHT RESTRICTIONS

This document may contain copyrighted materials. These materials have been made available for use in research, teaching, and private study, but may not be used for any commercial purpose. Users may not otherwise copy, reproduce, retransmit, distribute, publish, commercially exploit or otherwise transfer any material.

The copyright law of the United States (Title 17, United States Code) governs the making of photocopies or other reproductions of copyrighted material.

Under certain conditions specified in the law, libraries and archives are authorized to furnish a photocopy or other reproduction. One of these specific conditions is that the photocopy or reproduction is not to be "used for any purpose other than private study, scholarship, or research." If a user makes a request for, or later uses, a photocopy or reproduction for purposes in excess of "fair use," that user may be liable for copyright infringement.

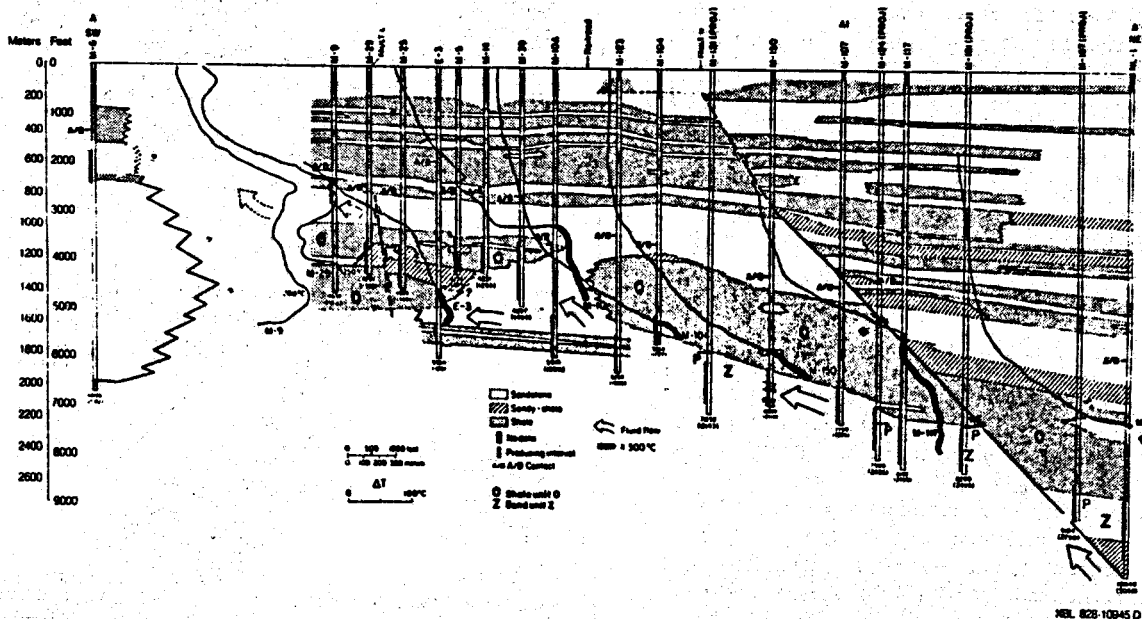
This institution reserves the right to refuse to accept a copying order if, in its judgment, fulfillment of the order would involve violation of copyright law.



NBL 864-10775

Figure 2. Location of some of the wells, principal faults, and cross section A-A' at Cerro Prieto.

Ubicación de algunos pozos, de las fallas principales y del corte transversal A-A' en Cerro Prieto.



NBL 828-10345 D

Figure 3. Lithofacies cross section A-A', showing well locations, lithofacies groups, faults, temperature profiles, producing intervals, A/B contacts, shale unit O, sand unit Z, and arrows indicating direction of fluid flow. On temperature profiles, points corresponding to 300°C are placed under the location of the respective wells. Parts of temperature profiles shown by heavy lines indicate temperatures 300°C or higher (from Halfman et al., 1984).

Corte transversal A-A' de litofacies, mostrando la ubicación de pozos, grupos de litofacies, fallas, perfiles de temperatura, intervalos de producción, el contacto A/B, la unidad lítica O, la unidad arenosa Z, y flechas indicando la dirección de flujo de los fluidos. Sobre los perfiles de temperatura, los puntos correspondientes a 300 °C están ubicados debajo de los respectivos pozos. Las partes de los perfiles de temperatura indicadas con líneas gruesas corresponden a temperaturas iguales o mayores de 300 °C (de Halfman et al., 1984)

ing to the α reservoir, rise up Fault L, and flow westward through the shallower sandstone [between M-29 and M-9 (800 - 1000 m)]. Eventually the geothermal fluids either mix with local cold groundwaters or discharge to the surface by way of the abundant manifestations present in the area, especially to the west and north of the wellfield.

Following Halfman et al.'s hydrogeological model, Figure 4A shows the geothermal fluid flow in the Cerro Prieto system schematically. The postulated fluid flow pattern is consistent with mineralogic (Elders et al., 1981, 1984), thermal (Mercado, 1976), and reservoir engineering and geochemical (Grant et al., 1984) studies conducted on the Cerro Prieto field. With exploitation the fluid flow pattern in the system, especially in western part of the field has changed. Colder groundwaters enter into reservoir through the western boundary and flowing down Fault L directly into the α reservoir (Fig. 4B). This reversal in local flow direction is indicated by the cooling of some wells, the decrease of chloride content in the produced fluids and by the progressive disappearance of surface manifestations (Truesdell and Lippmann, 1986). There are also evidences of colder water influx into the different reservoirs in other areas of the field.

Lippmann and Bodvarsson (1983) developed a two-dimensional numerical model of the field based on a portion of Halfman et al.'s (1984) hydrogeologic model. They obtained a good match with the observed natural-state pressures and temperatures. However, because of the two-dimensional nature of the model (not allowing recharge of the system along a horizontal direction perpendicular to the cross section that was modeled), a good pressure match for the 1973-1979 exploitation period was not possible.

Halfman et al. (1986a) extended the previous model to three dimensions, but only preliminary results were presented. The model discussed here includes an expanded 3-D computational mesh to obtain a more detailed description of the natural state conditions in the system, and computes the changes in reservoir pressures and temperatures/enthalpies after March 1973 when large-scale fluid production began at Cerro Prieto.

METHODOLOGY

The LBL three-dimensional, multi-phase simulator MULKOM (Pruess, 1988) was used to compute the heat and mass flow in the system.

First, a natural steady-state model of Cerro Prieto was developed. It was calibrated by varying the rock properties and boundary conditions of the model until reasonable matches between calculated and observed temperatures (Rivera et al., 1982; M.A. Ayuso, personal communication, 1988) and pressures (M.A. Ayuso, personal communication, 1988) were obtained. After that, the 1973-1987 exploitation of the field was simulated. The results of the model were compared against the observed reservoir pressure and enthalpy changes (Bermejo et al., 1979; M.A. Ayuso, personal communication, 1988).

Computational Mesh

The three-dimensional computational mesh incorporates the most important geologic features that control the flow of

fluids and heat in Cerro Prieto. These are, the lithology (permeable sandy layers and less permeable shales) and the normal Faults H and L (Halfman et al., 1984; Figs. 5 and 6). The NE-SW sides of the model are oriented parallel to the strike of Fault H (Fig. 5). The zone labeled Fault H in this figure represents the location of this fault in the model at the depth of the β reservoir. Fault H zone divides the mesh into two sections, the upthrown block to the NW and the downthrown block to the SE. The NW-SE sides of the model are approximately parallel to Fault L.

The horizontal dimensions of the mesh are 9000 m (NW-SE) by 8600 m (NE-SW) and includes the wellfield and surrounding areas. The mesh extends over the 800 and 4000 m depth interval. The computational mesh has been increased from 377 elements in the previous model (Halfman et al., 1986) to 401 elements in this model (228 internal and 173 boundary elements) and 740 connections between elements.

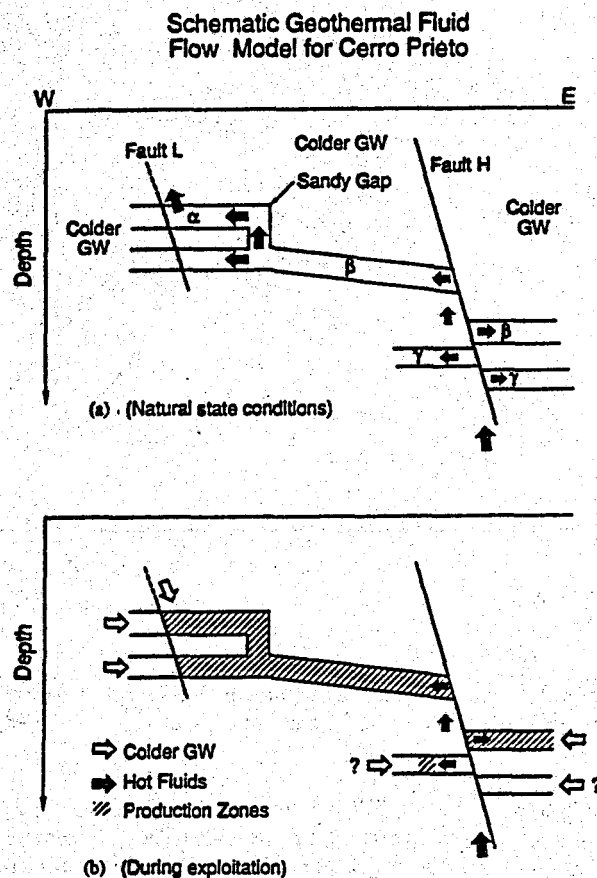


Figure 4. Schematic west-east cross section of the Cerro Prieto field showing geothermal fluid flow and cold groundwater (GW) recharge (a) prior to and (b) during exploitation (from Lippmann et al., 1989).

Corte transversal esquemático oeste-este del campo de Cerro Prieto indicando el flujo del fluido geotérmico y la recarga de agua subterránea (GW) fría, (a) antes y (b) durante la explotación (de Lippmann et al., 1989).

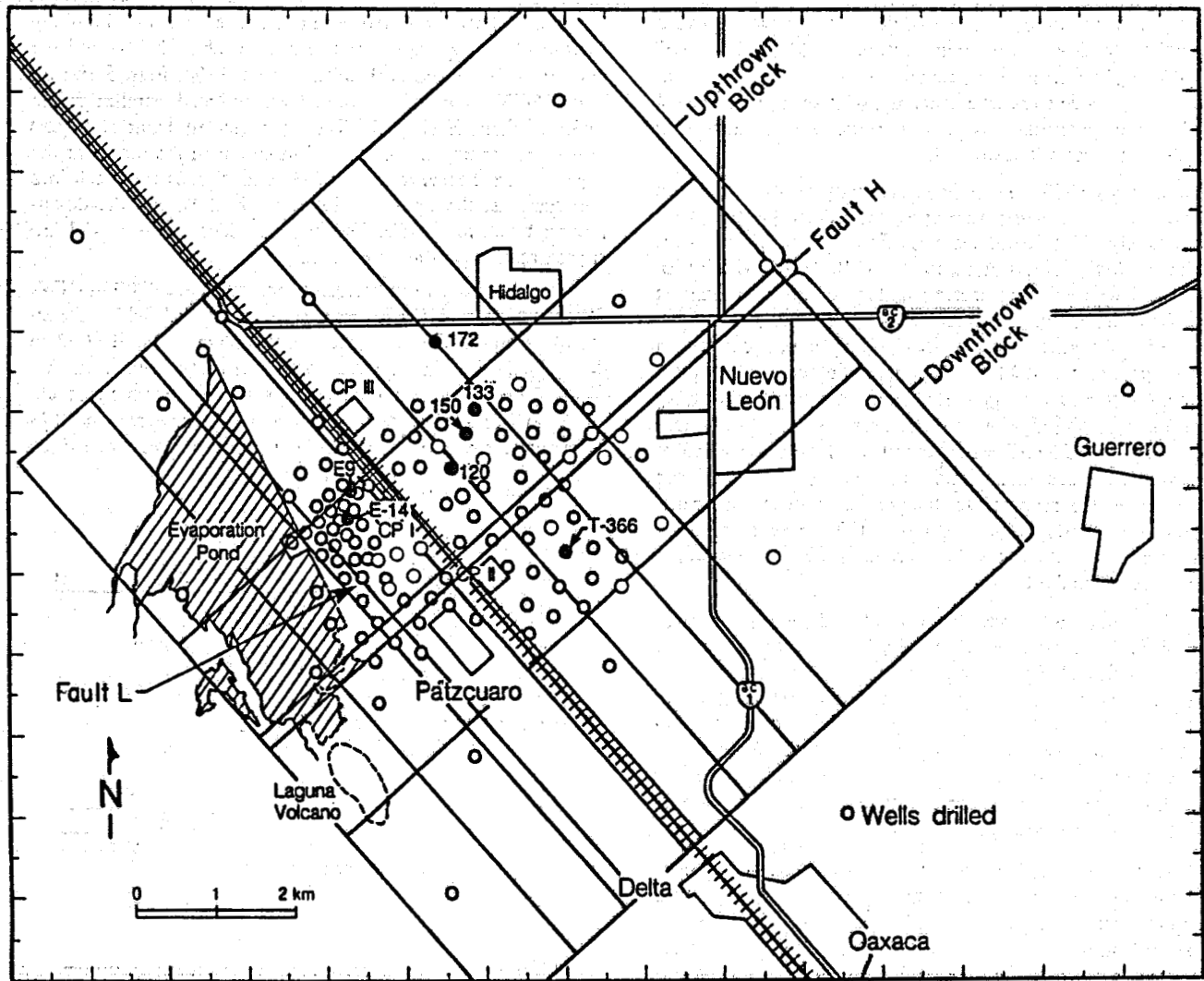


Figure 5. Plan view of the computational mesh used in this study.

XBL 849-9922B

Vista en planta de la malla de cómputo utilizada en este estudio.

Elements were added to the upthrown β reservoir to more accurately model the pressure and enthalpy changes observed in the field.

Figure 6 depicts a SW-NE cross section of the upthrown block showing the internal elements only. The mesh incorporates details of the subsurface geology, including the location of the three most permeable units (reservoirs α , β , and γ). Cross sections of the downthrown block have similar configuration. The blank elements represent permeable zones and the hatched ones low permeability zones. The recharge of geothermal fluids into the field is modeled by injecting hot 350°C fluids into the deepest easternmost element of the Fault H zone (not shown in Fig. 6). Most of this fluid ascends along the fault and flows westward and laterally through the various permeable zones. It discharges mainly along the upper southwestern boundary node on the upthrown element nearest the fault zone.

Material Properties

In the first simulation runs the rock properties assigned to the various mesh zones were similar to the ones used by Lippmann and Bodvarsson (1983). These material properties (especially permeabilities and thermal conductivities) were adjusted as the modeling work progressed, in order to match the observed and computed temperatures and pressures. Table 1 and Figures 7A and 7B shows the rock properties used in the best model, that is, the model that gave the best matches between observed and calculated values.

Figure 7A indicates the materials assigned to the elements in the SW-NE cross section of the upthrown block shown in Figure 6. The S1 zone represents a cooler aquifer overlying the geothermal field. A series of sandstones (SK1) and shales (CK1, CK2) represent the lithology inferred west of the geothermal anomaly. There is leaky cap rock (C1) above the α reservoir (S2). The western β reservoir (zones S3 and S3B) is separated from the α reservoir by a low permeability shale

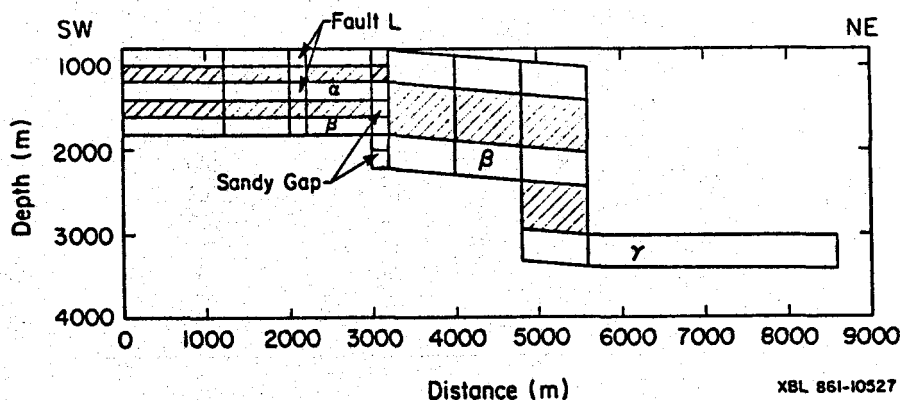


Figure 6. Southwest-northeast cross section through the grid elements just north of the Fault H. Hatched zones represent layers of lower permeability.

Corte transversal SO-NE mostrando los elementos de la malla ubicados al norte y junto a la Falla H. Las zonas rayadas representan capas de baja permeabilidad.

(C2). The sandy gap (S7) corresponds to zone of higher permeability connecting the β and α reservoirs. C5 zone represents an impermeable barrier believed to be caused by mineral precipitation, the result of the interaction between shallow, cooler groundwaters and the upflowing geothermal fluids (Lippmann and Bodvarsson, 1983). The eastern β reservoir (S5) is capped by the impermeable shale (C4), which is overlaid by a permeable sandstone (S4). A low-permeability shale (C6) separates the sandstones of the γ reservoir (S6) from the upper β reservoir.

In general, the lithology of the upthrown and downthrown sections is very similar (Figs. 7A and 7B). However, in the downthrown block the α reservoir, the westernmost part of the β reservoir (material S3 in Fig. 7A) and the sandy gap are not found. In this block these zones are shallier and less permeable than in the upthrown block and are represented by material C7.

The results of the best model indicates that the permeability of the sandy materials varies between 1 and 100 md and that of the shale layers between .005 and 1 md (Table 1). The horizontal permeability of the three reservoirs (α , β , and γ) is 100 md, while the vertical value is between 1 and 10 md. These permeabilities agree reasonably well with the results of well tests and with values used in earlier simulations of the field (Lippmann and Bodvarsson, 1983; Ayuso, personal communication, 1988). A constant rock density of 2650 kg/m^3 was used for all materials. Thermal conductivities ranged from of 2.35 to $3.00 \text{ W/m}^\circ\text{C}$, depending on rock type (these values are somewhat high especially for shaly materials, however that effect on the results are minimal).

Boundary Conditions

Constant temperature and pressure boundary elements are located along all sides of the computational mesh (i.e., surrounding the internal elements), except in some areas along the bottom. The temperatures assigned to the boundary elements

were based on normal temperature gradients for this area. The pressure assigned to the upper boundary elements (along the westernmost row of elements) of the upthrown and fault zone is 73 bars (800 m depth); and those of the downthrown section, 111 bars (1200 m depth). Below the γ reservoir and the eastern portion of the β close to the fault, the boundary conditions are simulated by including heat sources equivalent of 1 to 3 watts per square meter of interconnection area into the nearby internal elements. These sources simulate the heat flux associated with the cooling of igneous dikes believed to have intruded into the sedimentary fill of the Mexicali Valley (Elders et al., 1984; Goldstein et al., 1984).

In general, the boundary elements along the top of the mesh represent an impermeable shale, except along the extreme southwestern side where a permeable sandstone exists. Most of the lateral boundary elements to the southeast, southwest, and northwest have the same permeabilities as the internal elements they are connected to. The main exceptions are for a few of the boundary elements to the northwest, which are considered to be impermeable barriers because of mineral precipitation resulting from the interaction between different waters. Most of the boundary elements to the northeast are impermeable, except along the top row of the up- and downthrown sections where they represent a permeable sandstone. Impermeable boundary elements serve the purpose of accounting for conductive heat transfer.

Natural State Model

The natural state model provides quantification of the fluid (and heat) movement, and the distribution of temperatures, pressures, and steam saturations in the system before commercial fluid production started in March 1973. The validity of the model is supported by comparison to the geothermal fluid flow pattern inferred by the hydrogeologic study of Halfman et al. (1984) and the reasonable match obtained with best known initial temperatures and pressures at Cerro Prieto (Bermejo et al., 1979; and F.J. Bermejo, personal communication, 1982; M.A. Ayuso, personal communication, 1988.)

Table 1. Properties of the materials assigned to the zones used in the model, as shown in Figure 7A and 7B

Zones	Porosity (%)	Permeability (md)	
		horizontal	vertical
SK1,S1,S2,S3,S4,S3B	16	100	10
S5,S6	14	100	1
S7	14	100	5
CK1,C1,C2,C6	22	1	0.1
CK2,C4,C7,C8	25	.5	.005
C5	25	10	.005
F1	14	50	50

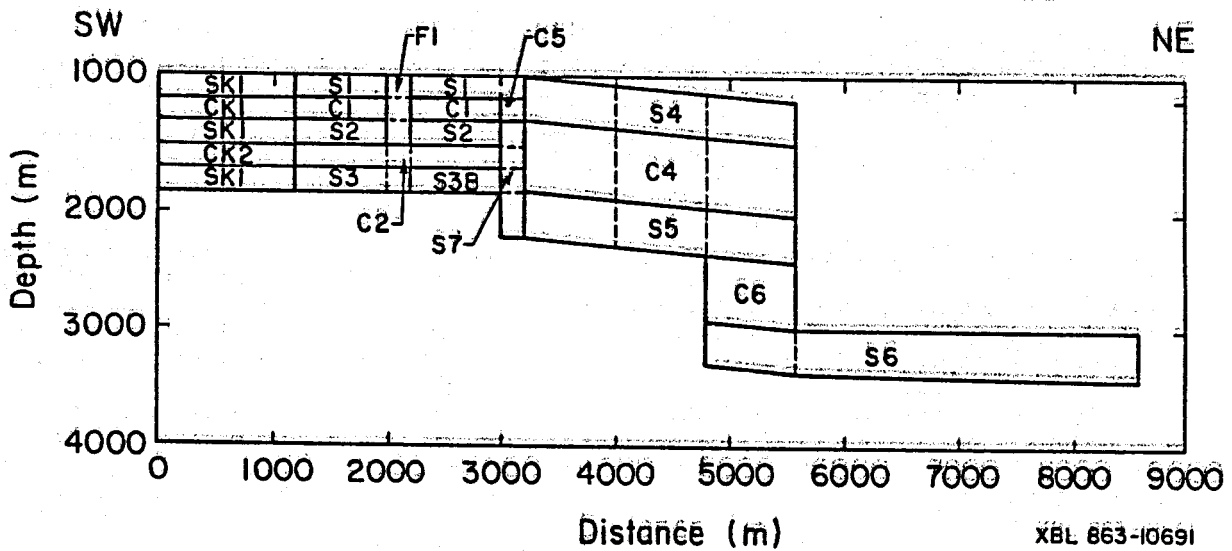


Figure 7A. Cross section given in Figure 6 showing different materials assigned to the upthrown block.
Corte transversal dado en la Figura 6 indicando los diferentes materiales asignados al bloque levantado.

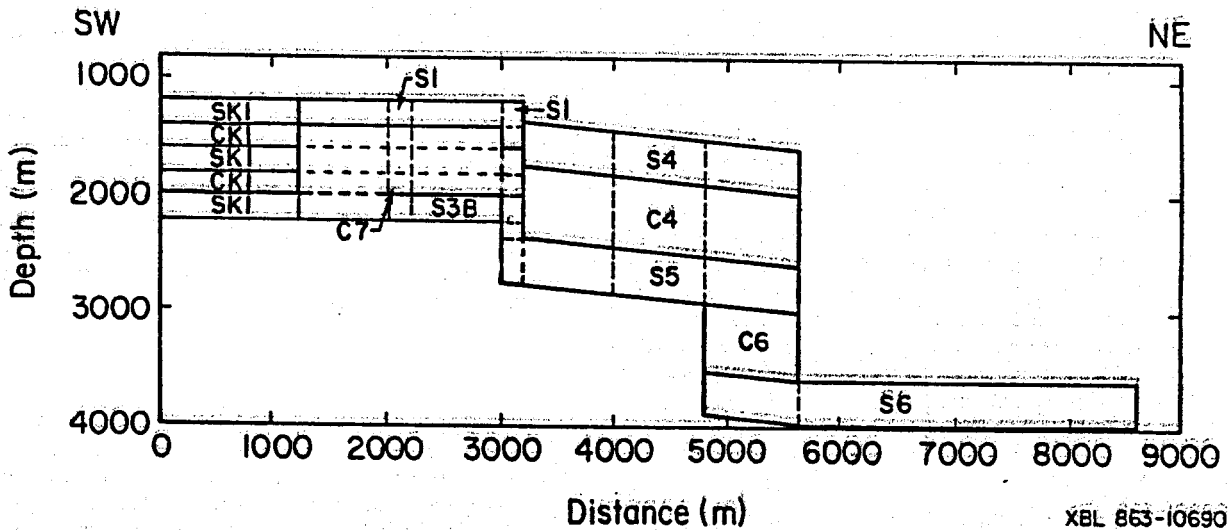


Figure 7B. Cross section through the southernmost SW-NE row of elements representing different materials assigned to the downthrown block.
Corte transversal a través de la hilera SO-NE más meridional de elementos, indicando los diferentes materiales asignados al bloque hundido.

Temperatures

Figures 8A and 8B represent the observed and calculated temperature distribution along the section given in Figure 6 (upthrown block). Both figures show the same general features. East of the sandy gap, the temperatures match fairly well. Both indicate a high thermal gradient in the cap rock zone (C4 of Fig. 7A) indicative of conductive heat flow. The main discrepancy in this area is in the uppermost element east of the sandy gap. The computed temperatures here are somewhat high. The model shows a small portion of the geothermal fluids flowing from the SW to the NE along the uppermost row of elements, instead of being entirely to the west as inferred by Halfman et al. (1984). The dashed isotherms shown west of

the sandy gap correspond to an area where the initial temperatures are not well known; there are data from only three wells (Fig. 8A). Well O-473 located in the southwesternmost column of elements in the mesh, has relatively cool temperatures. Well M-105 located to the south, in the second column of elements from the SW, has temperatures reaching 300°C at about 1400 m. Well M-181, a centrally located well in the same set of elements, also has these high temperatures at similar depths. According to this data the calculated temperature (300°C) is approximately 50°C too low in this region (Fig. 8B). However, Figure 17 of Bermejo et al. (1979) shows that downhole temperatures in well M-181 never exceed 275°C. Also, Mercado (1976) shows temperatures less than 300°C in

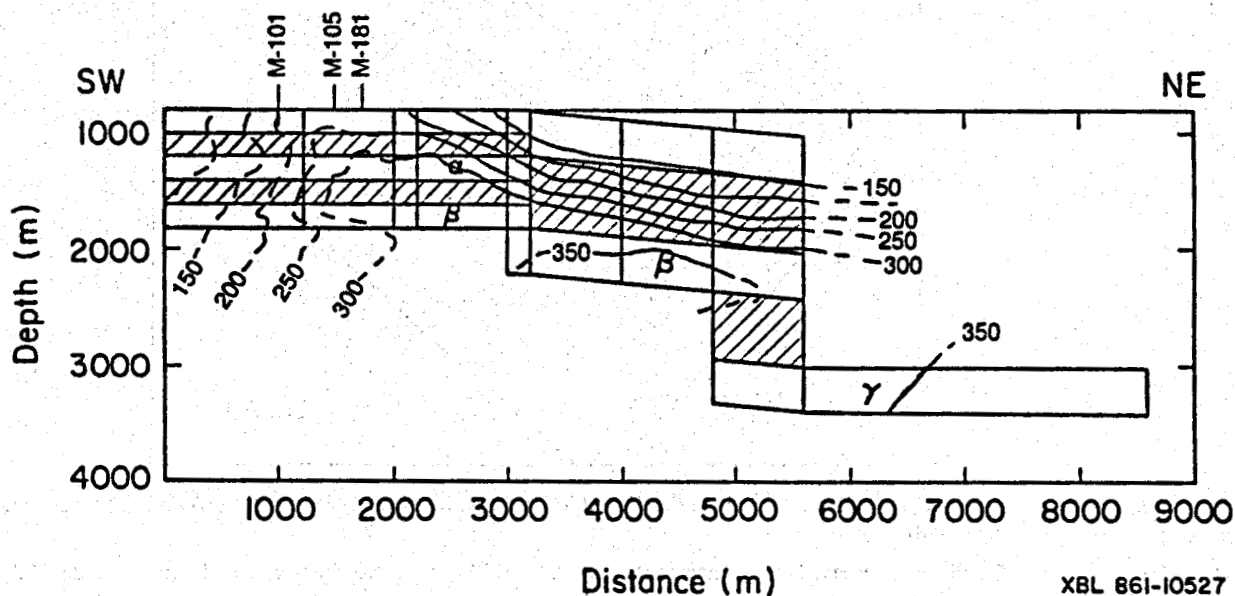


Figure 8A. Cross section given in Figure 6 showing observed temperature distribution (in °C).

Corte transversal dado en la Figura 6, mostrando la distribución observada de temperaturas (en °C).

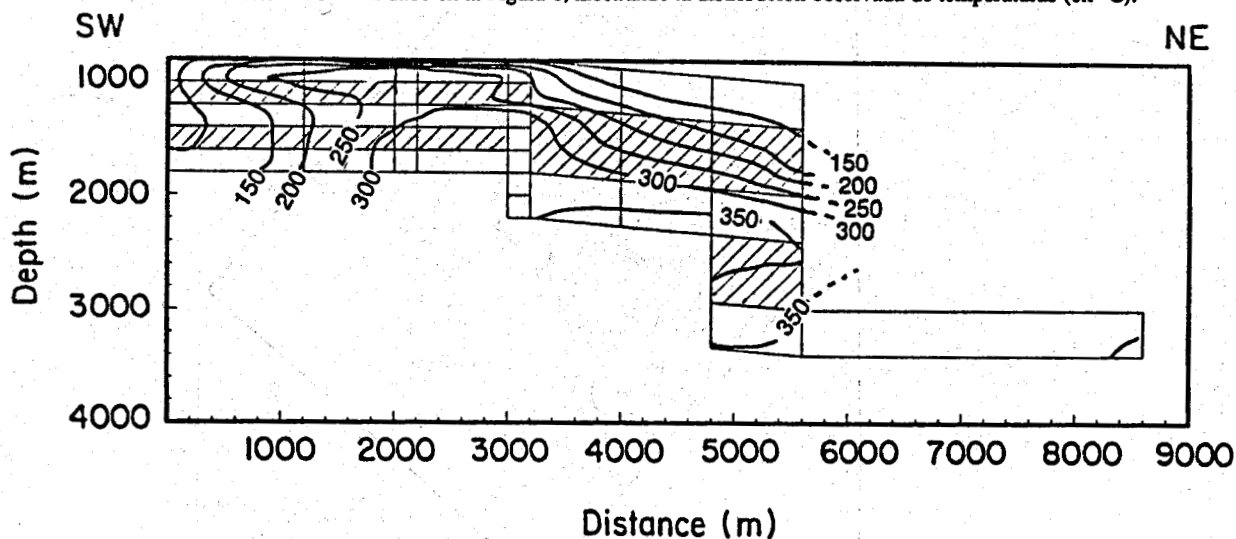


Figure 8B. Cross section given in Figure 6 showing calculated temperature distribution (in °C).

Corte transversal dado en la Figura 6, mostrando la distribución calculada de temperaturas (en °C).

this general region of the field. Therefore, we consider our calculated temperature distribution in the vicinity of M-181 to agree reasonably well with measured downhole data.

Figures 9A and 10A show the observed temperature distributions for the α reservoir (1300 m depth) and the western β reservoir (1700 m depth), respectively. The isotherms were

plotted using well log data (M.A. Ayuso, personal communication, 1988) and the calculated temperatures for normal thermal conditions along the boundary of the mesh. The dots represent the data points (location of wells) used to generate the plots. For comparison, Figures 9B and 10B show the computed temperature distributions.

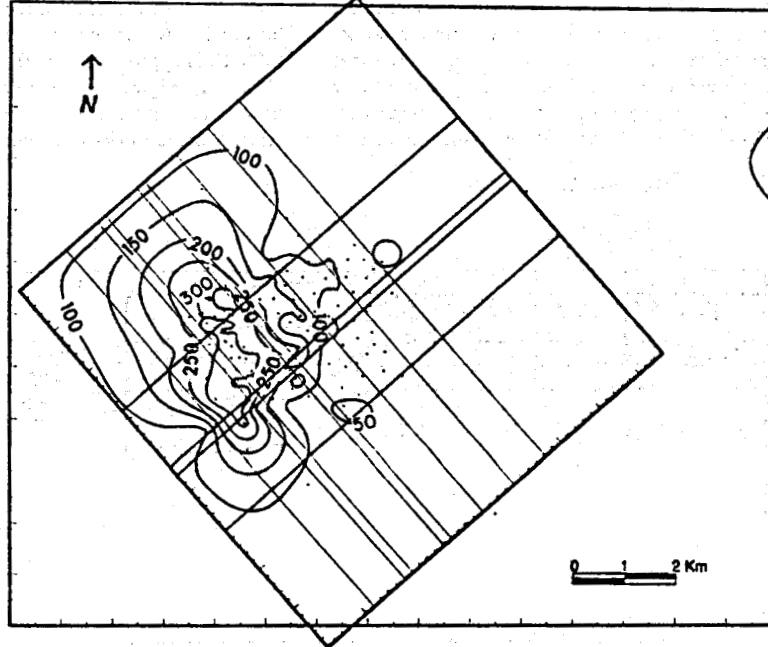


Figure 9A. Observed temperature distribution (in °C) at 1300 m depth, based on data from M. A. Ayuso (personal communication, 1988).

Distribución observada de temperaturas (en °C) a 1300 m de profundidad, basada en datos de M.A. Ayuso (comunicación personal, 1988).

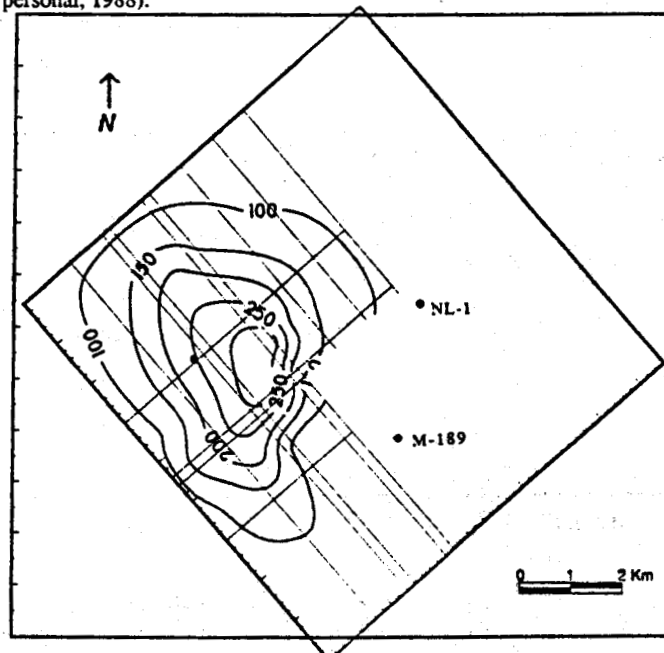


Figure 9B. Calculated temperature distribution (in °C) at 1300 m depth.

Distribución calculada de temperaturas (en °C) a 1300 m de profundidad.

1300 m depth (Fig. 9). The observed and computed temperature distributions at the 1300 m depth level match fairly well. Both figures show an elongation of the isotherms in a NE-SW direction. At this level, the hotter part of the field corresponds to the α reservoir, here considered to be at an average depth of 1300 m. At first glance, the computed 300°C isotherm appears to be somewhat displaced east of the observed temperatures, which show two 300°C closed contours (Figure 9A). One should note that most of the wells between the two closed contours and directly to the east of the larger one, have temperatures that are quite close to 300°C. Therefore, the position of the eastern edge of the computed 300°C isotherm is quite reasonable. Toward the west, this isotherm does not extend as far as observed in the field. The western edge of the observed 300°C isotherm is mainly based on two wells with disputed temperature profiles (wells M-181 and M-105); the reported downhole values seem to be high for 1300 m depth. Therefore, it is questionable whether the 300°C contour really extends over such a wide area in the western part of the field. In general, although the calculated area enclosed by this contour is somewhat too large, it is a fairly good approximation of the observed temperatures, especially if one considers the size of the elements in the computational mesh.

To the east of the railroad tracks, the calculated isotherms at 1300 m depth extend farther east than the observed ones. This is due to the anomalous northeastern flow of geothermal fluid shown in the model (discussed above) along the top row of elements. Future simulations will rectify this situation.

1700 m depth (Fig. 10). In general, at 1700 m depth along the Fault H, the regions bounded by the isotherms tend to narrow in the eastern region of the field and spread out in the western

part (Figs. 10A and 10B). The core of the producing western β reservoir is included in the 300°C closed isotherm.

In the observed temperatures (Fig. 10A) the upflow of hot fluids along Fault H is evident by the closely spaced contours parallel to the fault zone, east of the sandy gap. Although the computed temperature distribution (Fig. 10B) does not show as striking example of this phenomena, it still is evident by the convergence of the isotherms and their trend parallel to the fault. (The size of the mesh limits the resolution of sharper temperature gradients.)

Pressures

Figures 11 and 12 show the calculated and observed pressures for 1300 and 1700 m depth, respectively. At 1300 m, most of the observed values do not correspond to open intervals in the wells, therefore they must have been calculated by interpolation or extrapolation. The observed values show increasing pressures toward the center of the mesh, ranging from 122.3 to about 126 bars. The calculated pressures differ by only a few bars (Fig. 11), and show a similar trend, varying over the field between 121 and 127 bars.

The observed and calculated pressures at 1700 m show very small differences (up to 2 bars; Fig. 12). In the northeastern section of the downthrown block the 157 and 158 bar contours correspond quite closely.

Geothermal Circulation and Boiling

The three-dimensional numerical model for the natural state shows a fluid circulation pattern that corresponds to that of Halfman et al.'s (1984) hydrogeologic model discussed ear-

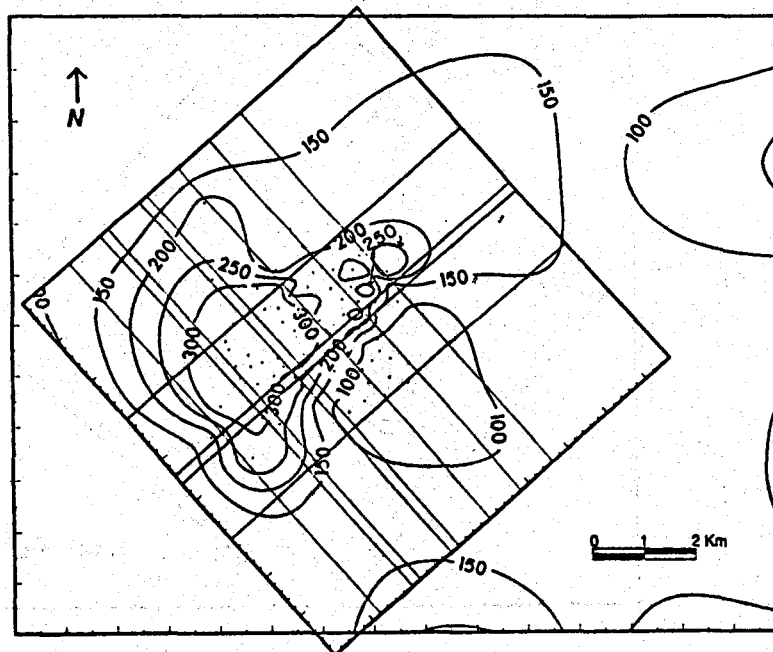


Figure 10A. Observed temperature distribution (in °C) at 1700 m depth based on data from M. A. Ayuso (personal communication, 1988).

Distribución observada de temperaturas (en °C) a 1700 m de profundidad, basada en datos de M.A. Ayuso (comunicación personal, 1988).

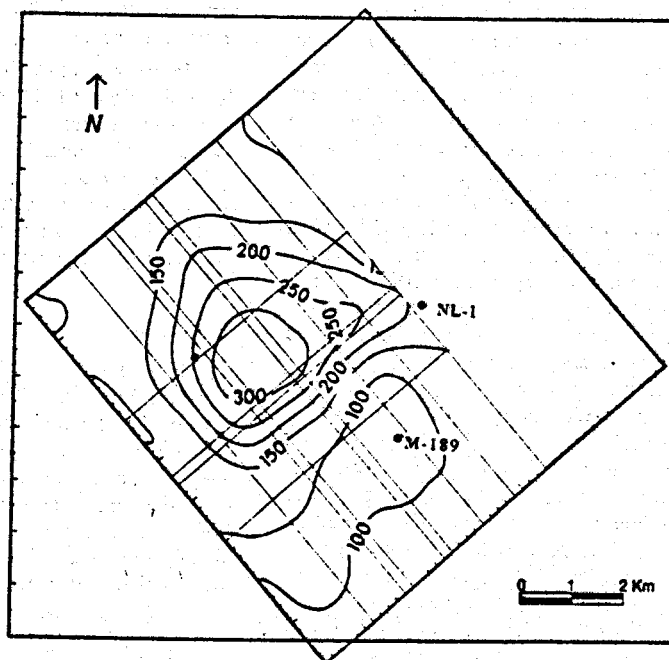


Figure 10B. Calculated temperature distribution at 1700 m depth.
 Distribución calculada de temperaturas (en °C) a 1700 m de profundidad.

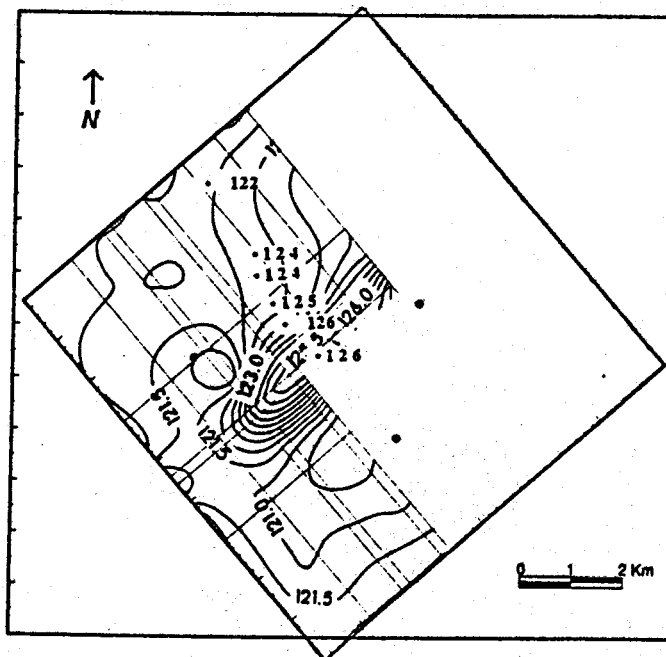


Figure 11. Observed (M. A. Ayuso, personal communication, 1988) pressure data (shown as dots) with pressure values and contours of calculated pressure at 1300 m.
 1300 m de profundidad. Presiones observadas indicadas por los puntos (M.A. Ayuso, comunicación personal, 1988); los contornos corresponden a presiones calculadas.

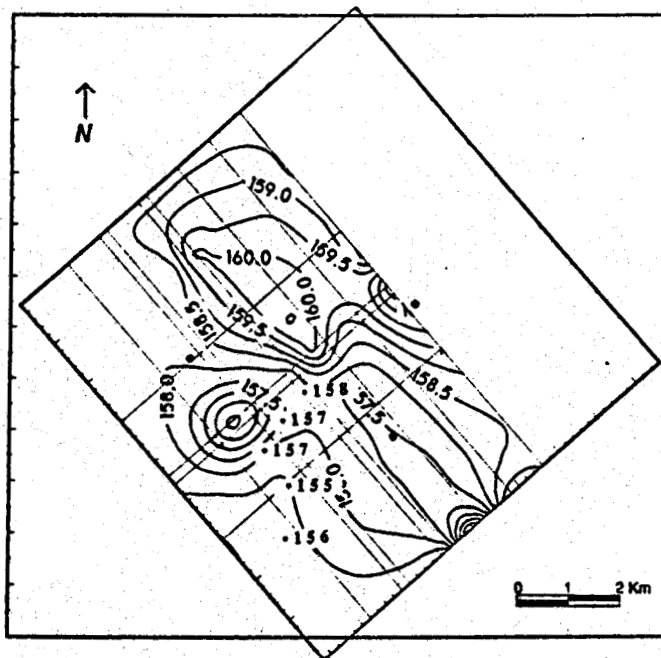


Figure 12. Observed (Ayuso, personal communication, 1988) pressure data (shown as dots) with pressure values and contours of calculated pressure at 1700 m.

1700 m de profundidad. Presiones observadas indicadas por los puntos (M.A. Ayuso, comunicación personal, 1988); los contornos corresponden a presiones calculadas.

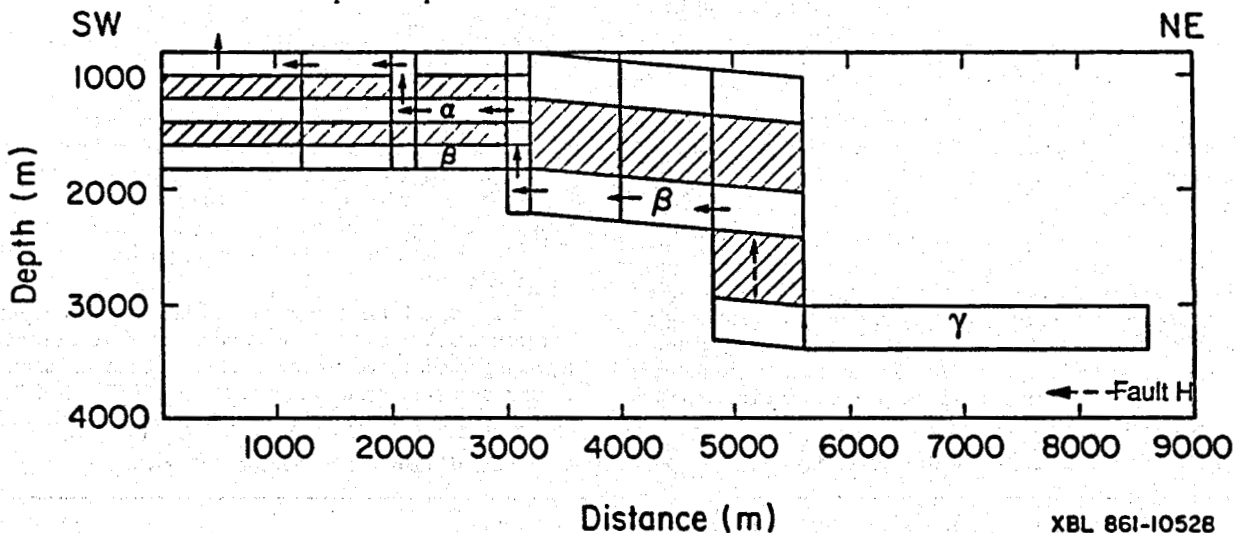
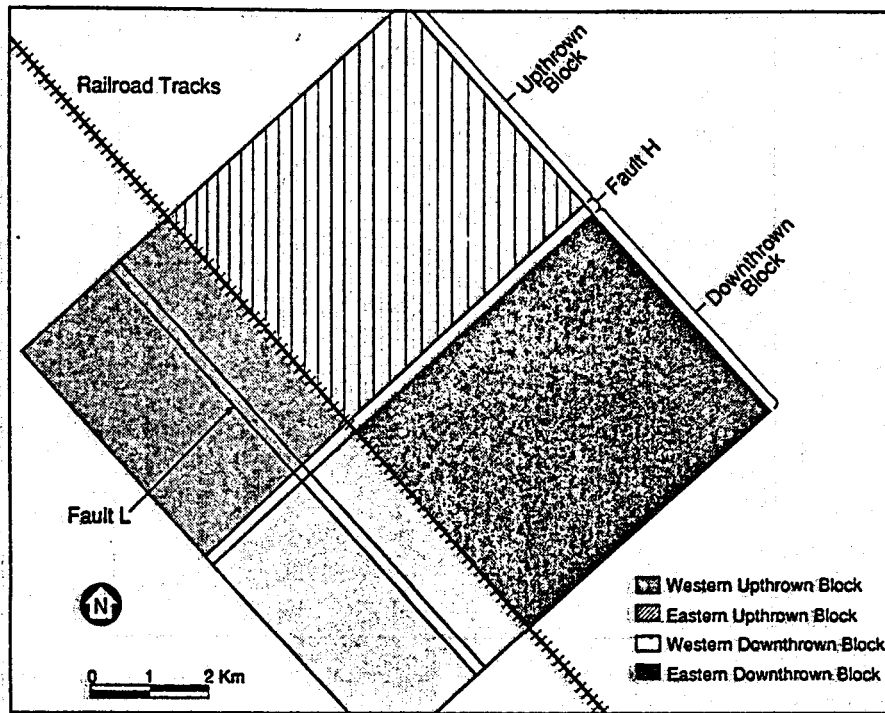


Figure 13. Generalized fluid flow pattern for the cross section shown in Figure 6. The dashed arrow between the β and γ reservoirs indicates vertical flow in the fault zone (located to the southeast).

Patrón generalizado de flujo del fluido correspondiente al corte transversal dado en la Figura 6. La flecha punteada entre los yacimientos β y γ indica el flujo vertical en la zona de falla (ubicada al sudeste).

lier (Fig. 13). For the best model, a constant 80 kg/s recharge rate of 350°C (1671 kJ/kg enthalpy) water was computed; source located in the deepest easternmost element of the Fault H section. The model shows that geothermal fluids rise along the Fault H zone. A small amount of fluid enters the sandstones of the γ reservoir (Figure 13), but most of the fluids move upward along the fault and then migrate laterally and westward into the sandstones of the β reservoir. From the β reservoir the

fluids move into the sandy gap where some boiling occurs and continue to flow westward through the α reservoir. Our natural state model indicates that the α reservoir is also recharged with fluid flowing directly from Fault H (this differs with the hydrogeologic model that indicates geothermal fluids recharge only from the sandy gap). From the α reservoir the fluids ascend up Fault L, moving westward through the shallow aquifer and then eventually migrate to the surface along the westward edge



XBL-693-7530

Figure 14. Simplified plan view of the computational mesh (Fig. 5) showing the western upthrown, eastern upthrown, western downthrown, and eastern downthrown blocks.

Vista en planta simplificada de la malla de cómputo (Fig. 5) indicando los bloques occidentales y orientales, elevados y hundidos.

of the field. Figure 13 shows only a schematic of the flow pattern because of the three-dimensional nature of the model.

Exploitation Model

In the second phase of this numerical modeling study, fluid production at Cerro Prieto was simulated between 1973 and 1987; the Halfman et al. (1986a) study only considered production up to 1979. Actual production data from individual wells (provided by CFE) was simulated by assigning appropriate fluid sinks to various mesh elements. Computed pressure and enthalpy changes in the α and β reservoirs were compared against observed values.

Table 2 lists the average annual fluid production rates for the various geothermal reservoirs and zones in and near Fault H and L that were incorporated into the model. The α reservoir was the first to be exploited; and its exploitation continues today. Production from the β reservoir started in 1978. Presently, the bulk of the fluid is being produced from this deeper reservoir.

In the model, the β reservoir has been subdivided into four sections. A given area is assigned to one of these sections depending whether it is east or west of the railroad tracks, or in the upthrown or downthrown block of Fault H (Fig. 14). The eastern upthrown section roughly corresponds to CPIII in the

Table 2. Production rates (in kg/sec) for the different areas of the Cerro Prieto field for the 1973-1987 period

Reservoirs / Zones	Years														
	73	74	75	76	77	78	79	80	81	82	83	84	85	86	87
α	349.9	450.5	465.7	575.9	636.4	570.4	526.3	418.7	392.3	337.5	327.5	308.0	299.3	288.4	184.9
Uprthrown β (west)	-	-	-	-	-	6.2	233.3	207.6	247.7	399.7	409.3	357.4	372.6	469.6	280.1
Uprthrown β (east)	-	-	-	-	-	16.1	-89.7	70.3	-68.6	-67.0	-50.7	-62.8	105.5	840.1	551.9
Downthrown β (west)	-	-	-	-	-	-	69.3	83.9	76.3	92.2	100.7	87.4	141.3	168.5	103.4
Downthrown β (east)	-	-	-	-	-	-	-	-	-	46.6	49.1	30.0	2.3	938.8	632.8
Faults H and L	32.3	140.2	137.2	125.9	118.1	121.8	291.6	254.8	238.3	262.0	267.6	249.8	230.6	245.5	200.3
Total	382.2	590.7	602.9	701.8	754.5	714.5	1210.2	1035.3	1023.2	1205.0	1204.9	1095.4	1151.6	2950.9	1953.4

Tabla 2. Producción (en kg/seg) para las diferentes áreas del campo de Cerro Prieto, período 1973-1987.

northeastern area of the field, and the eastern downthrown section to CPII, in the southeast. In the model the western two sections of the β reservoir represent the up- and downthrown portions of this reservoir in CPI. To represent the eastern and western upthrown block of the β reservoir more accurately, a more detailed mesh than the one shown in Figure 2 was constructed.

The material properties and boundary conditions used for the exploitation model were identical to those of the natural state model. The hot water recharge (80 kg/s of 350°C water) into the deepest easternmost element of the Fault H section was assumed to be constant and unaffected by reservoir drawdown. The constant pressure and temperature boundaries were considered to be adequate for simulating the early exploitation history. These boundary conditions will have to be modified for predicting the later behavior of the Cerro Prieto system (i.e., after 1987).

In response to production-induced drawdown, the model indicated a rearrangement in the direction of fluid movement, similar to what is shown in Figure 4.

Response of the α reservoir. The reported observed 1973-1987 pressure for the α reservoir (M.A. Ayuso, personal communication, 1988; Bermejo et al., 1979) were often obtained by extrapolating and interpolating measurements from a few observation and temporarily shut-in production wells. For each year and particular area, the pressure for a representative well, or wells, were averaged and plotted for comparison against corresponding calculated values.

Figure 15 shows the observed and calculated pressures in the α reservoir at 1200 m depth. The solid curve represents the

pressures given by Bermejo et al. (1979) and the crosses represent reported well M-38 pressures. The solid curve shows for the 1973-1979 period a pressure drawdown of about 22 bars (from about 110 to 88 bars). On the other hand, well M-38 shows between 1973 and 1977 an initial drawdown of about 6 bars (from 97 to 91 bars), followed by pressure recovery. These results reflect the effects of changes in fluid production rates and an increasing influx of colder ground waters.

Pressures reported for other wells in the same area and for the same depth, are often higher than those of well M-38. For instance, in 1977 and 1978 these pressures were about 14 bars higher than those reported for M-38. We do not know the reason behind these differences.

The calculated pressures match the M-38 pressures quite closely (Fig. 15). Initially, the model shows a pressure drawdown, which starting about 1976 is followed by a partial recovery.

In the α reservoir the observed enthalpy histories vary from well to well, however in most wells enthalpies rarely exceed 400 kcal/kg (about 1675 kJ/kg). Some wells show fairly constant enthalpy values; other wells show a decrease. Finally, for a number of wells, higher enthalpies were observed in the mid 1970s, which then decreased and soon afterwards leveled off. We chose well M-26 out of this last group and considered it to represent the enthalpy behavior of the α reservoir (Fig. 16).

Figure 16 also shows the calculated enthalpy history for the main portion of the α reservoir between Fault L and the sandy gap. The model shows a decreasing trend in enthalpies. It agrees fairly well with the observed changes except around

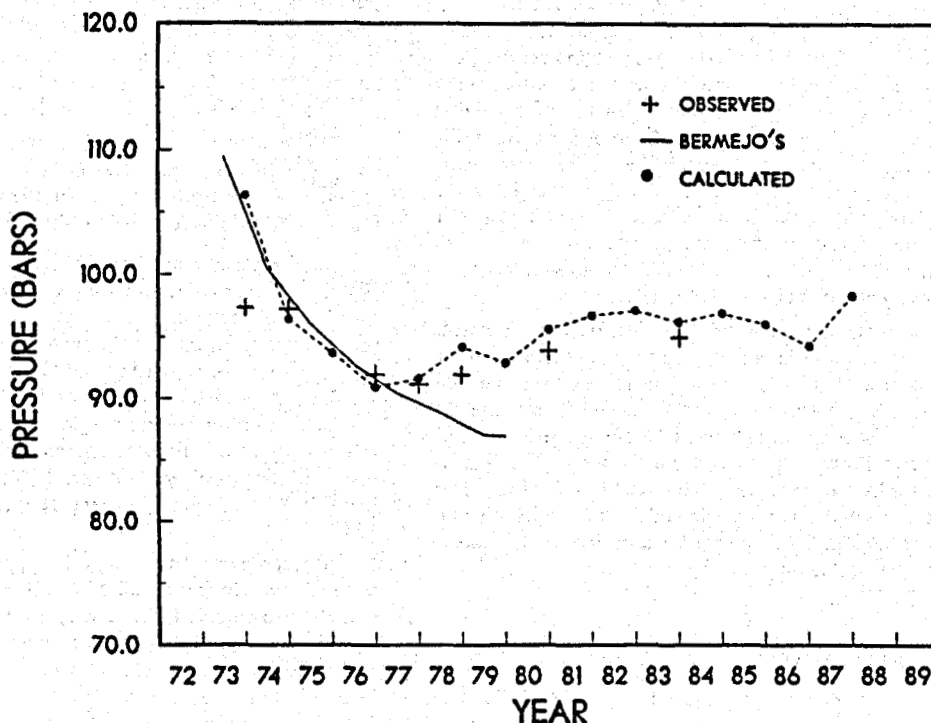


Figure 15. Observed (well M-38 and Bermejo et al.'s data, 1979) and calculated pressure histories for the α reservoir.

Historia de las presiones observadas (pozo M-38 y datos de Bermejo et al., 1979) y calculadas para el yacimiento α .

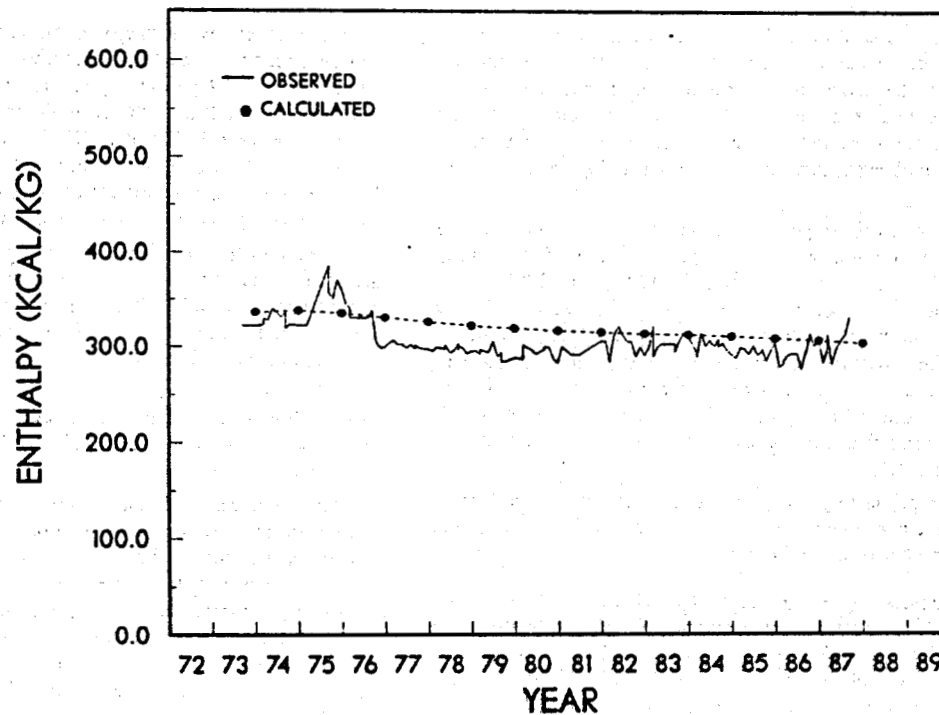


Figure 16. Observed (well M-26) and calculated enthalpy histories for the α reservoir.

Historia de las entalpías observadas (pozo M-38) y calculadas para el yacimiento α .

the 1975-1976 period, when higher enthalpies were observed associated with localized reservoir boiling (Truesdell et al., 1984, 1989; Lippmann et al., 1989). The elements of our 3-D computational mesh are much too coarse to simulate the boiling around wells, therefore our model does not show the higher enthalpies observed in the field, though in the model the α reservoir is on the verge of boiling. If the reservoir permeabilities are reduced by only five percent, the model shows intermittent boiling from 1974 to 1977. If the permeabilities are reduced by ten percent, the model indicates that the α reservoir boils continuously during the same period. So, even though our best model shows no boiling, the fact that it is on the verge of it, is consistent with field observations.

Cold water recharge through Fault L and from the west is reflected by a decrease in enthalpy starting about 1976, in the observed M-26 enthalpies and in the general decrease in calculated enthalpies. Unlike field data from which one infers a predominant recharge through Fault L, our numerical model shows most recharge originating from the west. This can be accounted for by the presence in the model of one of the sinks (simulated well) in the upper portion of Fault L, which disrupts the recharge through the fault into the α reservoir. The model will be modified in the future.

Responses in the β reservoir

Eastern upthrown block. Figure 17 shows the 1973-1987 observed and calculated pressures for the eastern upthrown block of the β reservoir (Fig. 14) at 2100 m depth. Between 1979 and 1982 the observed representative pressures for the

area near well M-150 (data from wells M-150 and M-133) show a slight decrease from 188 to 180 bars. Then they steeply decline to about 155 bars in 1986 (Fig. 17). This rapid and sudden decrease in pressure reflects the coming on line of power plant CP111, as production greatly increased from about 105 kg/sec in 1985 to 840 kg/sec in 1986 (Table 2).

The calculated and observed pressures match extremely well. The calculated pressures in the vicinity of M-150 show a pressure decline from 196 bars in 1973 to 178 bars in 1985, followed by a sharp decrease to 149 bars in 1986 (Fig. 17).

In the eastern upthrown block of the β reservoir, two slightly different trends are seen in the observed well enthalpy histories. In the main portion of this part of the producing field (north of Fault H, up to wells such as M-120 and M-150, Fig. 5), a trend toward increasing enthalpies is observed; up to 600 kcal/kg (about 2510 kJ/kg; e.g., well M-120, Fig. 18). The data indicates reservoir boiling due to stepped-up fluid production and the lack of significant fluid recharge into this portion of the reservoir (Semprini and Kruger, 1984; Stallard et al., 1987; Léon de Vivar, 1988; Lippmann et al., 1989; Truesdell et al., 1989).

Farther away from Fault H, approaching the northern edge of the field (near well M-133, Fig. 5), increasing enthalpies are also observed, but in this area the enthalpies are lower; they do not exceed 450 kcal/kg (about 1880 kJ/kg; e.g., well M-133, Fig. 19). The location of the northern boundary of the field is inferred by the sudden and sharp deepening of the 300°C isotherm, from about 2000 m in well M-133 to below 3800 m in M-172 (Halfman et al., 1986b), showing the hot fluids not migrating north much beyond well M-133. The

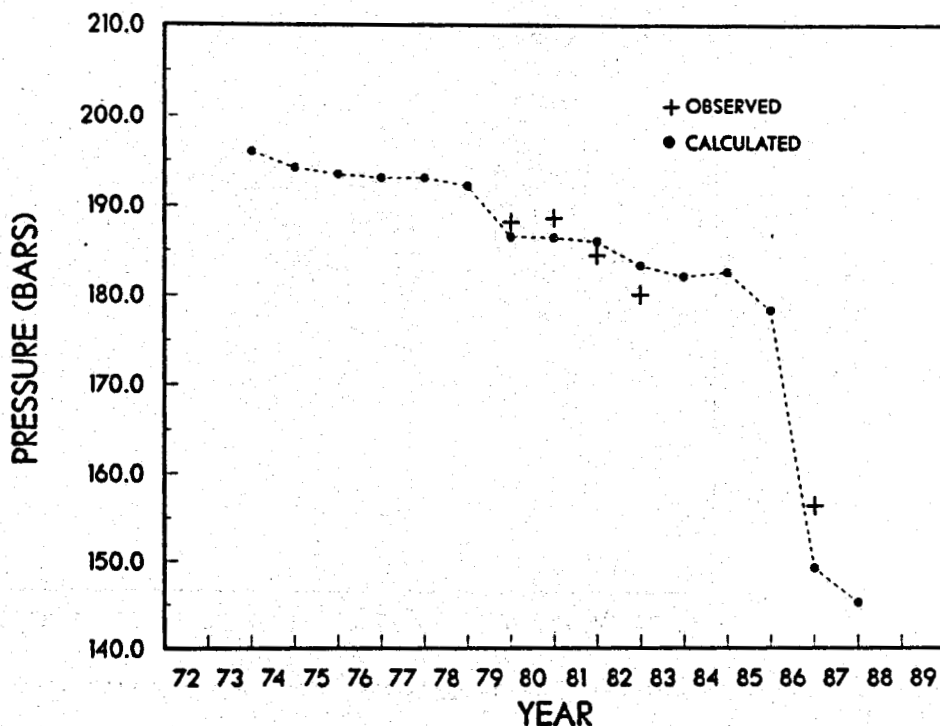


Figure 17. Observed (wells M-150 and M-133) and calculated pressure histories for the eastern upthrown block of the β reservoir.

Historia de las presiones observadas (pozos M-150 y M-133) y calculadas para el bloque oriental levantado del yacimiento β .

observed enthalpies indicate that reservoir boiling has occurred at least during 1986 and 1987. The lower observed enthalpies in this region as compared to the zone nearer to the fault, indicate that there is cold water recharge in this northern fringe area of the geothermal system.

For the portion of the eastern upthrown block of the β reservoir nearest to Fault H the calculated increases in enthalpy are slightly delayed with respect to the observed ones (Fig. 18). This delay can be explained by mesh discretization effects. The calculated enthalpies for this area tend to be constant between 1979 and 1985 (around 385 kcal/kg; about 1610 kJ/kg), and then start to increase in 1986 (Fig. 18). This trend reflects the boiling in the model starting in 1986.

In the region farther away from the fault (e.g., near well M-133) the calculated and observed enthalpies (well M-133) match well (Fig. 19). The enthalpies between 1978 and 1985 are constant (around 380 kcal/kg; about 1590 kJ/kg) and then rise to 460 kcal/kg (about 1925 kJ/kg) by 1988, the model shows reservoir boiling beginning in 1986.

Western upthrown block. Figure 20 shows the observed and calculated 1973-1987 pressures for the western upthrown block of the β reservoir at 1800 m depth. Prior to any production in the field (1973) the pressures were about 165 bars (adjusted pressure from 1700 to 1800 m depth; Fig. 12). The first reported representative pressure in the area near well E-9 (data from wells E-3, E-9 and E-14) after production started, was 144 bars in 1981, a drop of 21 bars from pre-exploitation conditions. The pressure fluctuated between 1984 and 1986

possibly in response to variations in annual fluid production rates (Table 2).

There is good agreement between the observed and computed pressures for 1985 and 1986, but the 1984 calculated pressure is 10 bars higher than the observed one. The calculated pressures shows a decrease from about 161 bars in 1973 to 157 bars in 1978 (Fig. 20) before significant production had occurred (Table 2). Then, with increasing production, the pressures dropped to 141 bars in 1983, and then began to fluctuate due to varying production rates.

Some wells in the western upthrown block of the β reservoir are characterized by increasing enthalpies, while others by their fairly constant values. The wells with increasing enthalpies are found in the main portion of this block; i.e. east of Fault L, west of the sandy gap, north of Fault H, and as far north as E-14 (Fig. 5). The enthalpy behavior of well E-2 (Fig. 21) is typical for this area. The enthalpies increase from about 360 kcal/kg (about 1505 kJ/kg) in 1984 to about 600 kcal/kg (about 2510 kJ/kg) in 1988, suggesting reservoir boiling starting around 1986. This boiling could be in response to an increasing overall exploitation of the β reservoir (Table 2), with natural recharge not keeping pace with production. León de Vivar (1988) and Truesdell et al. (1989) have also suggested reservoir boiling in this portion of the field.

Northwest of the area just described, i.e., west of Fault L and north of E-14, the enthalpies are fairly low and constant (generally less than 400 kcal/kg (about 1675 kJ/kg; e.g., well E-3, Fig. 22). The constant enthalpy shown by the wells in this

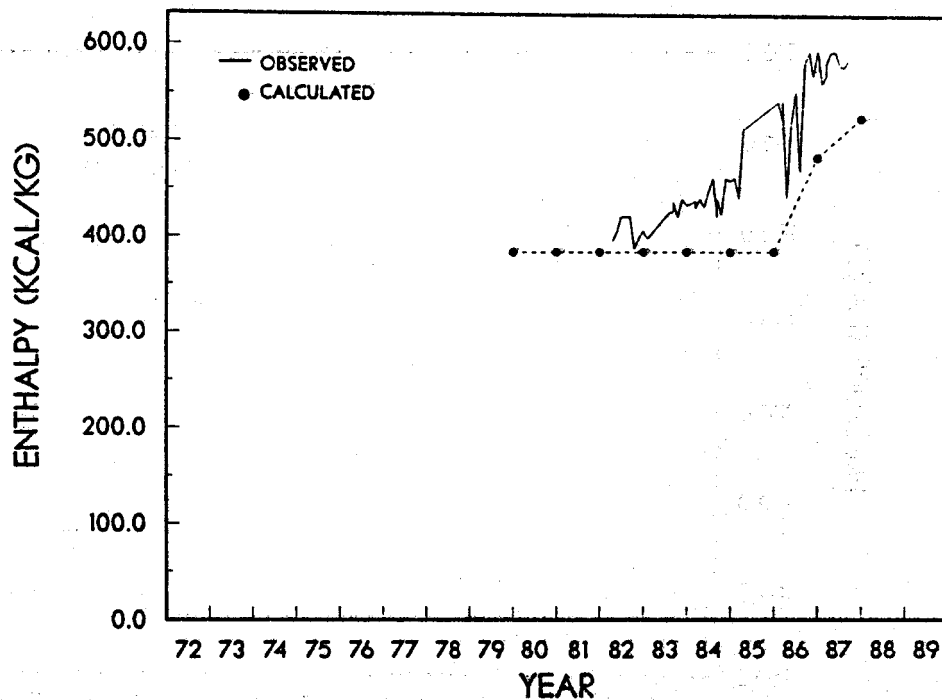


Figure 18. Observed (well M-120) and calculated enthalpy histories for the eastern upthrown block of the β reservoir near Fault H.

Historia de las entalpías observadas (pozo M-120) y calculadas para la zona cercana a la Falla H en el bloque oriental levantado del yacimiento β .

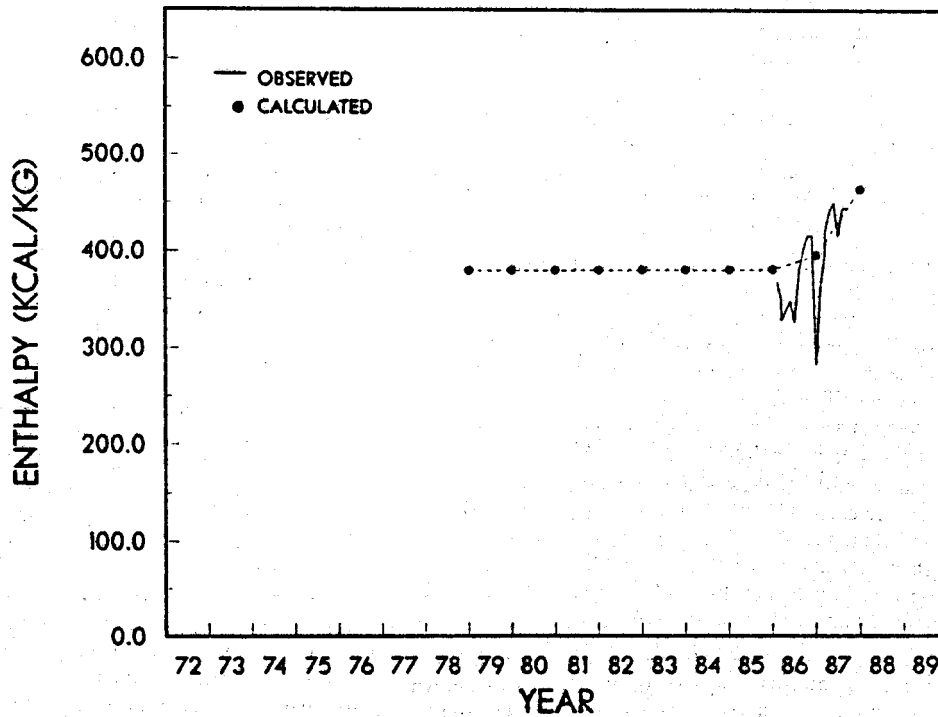


Figure 19. Observed (well M-133) and calculated enthalpy histories for the eastern upthrown block of the β reservoir farther to the north of Fault H (near M-133).

Historia de las entalpías observadas (pozo M-133) y calculadas para la zona distante y al norte de la Falla H, en el bloque oriental levantado del yacimiento β (cerca del M-133).

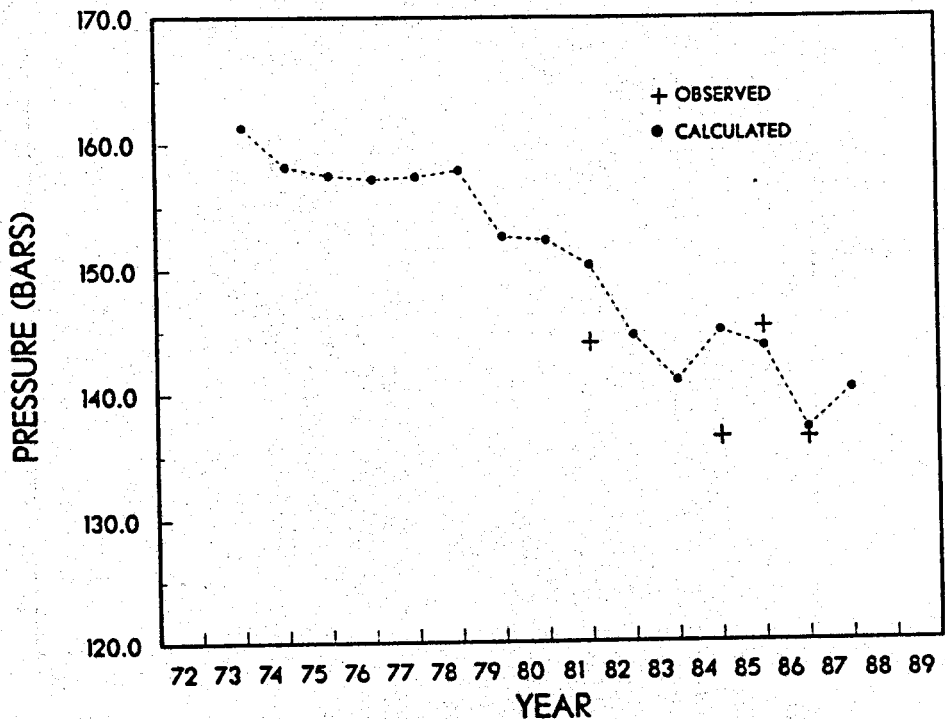


Figure 20. Observed (wells E-3, E-9, and E-14) and calculated pressure histories for the western upthrown block of the β reservoir.

Historia de las presiones observadas (pozos E-3, E-9 y E-14) y calculadas para el bloque occidental levantado del yacimiento β .

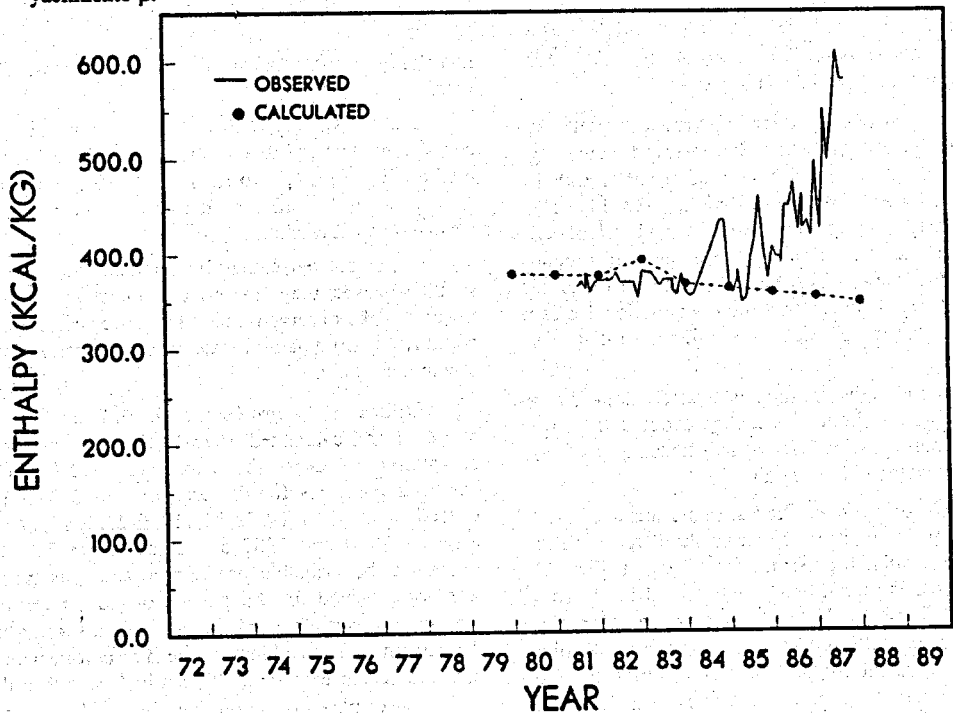


Figure 21. Observed (well E-2) and calculated enthalpy histories for the western upthrown block of the β reservoir near Fault H.

Historia de las entalpías observadas (pozo E-2) y calculadas para la zona cercana a la Falla H en el bloque occidental levantado del yacimiento β .

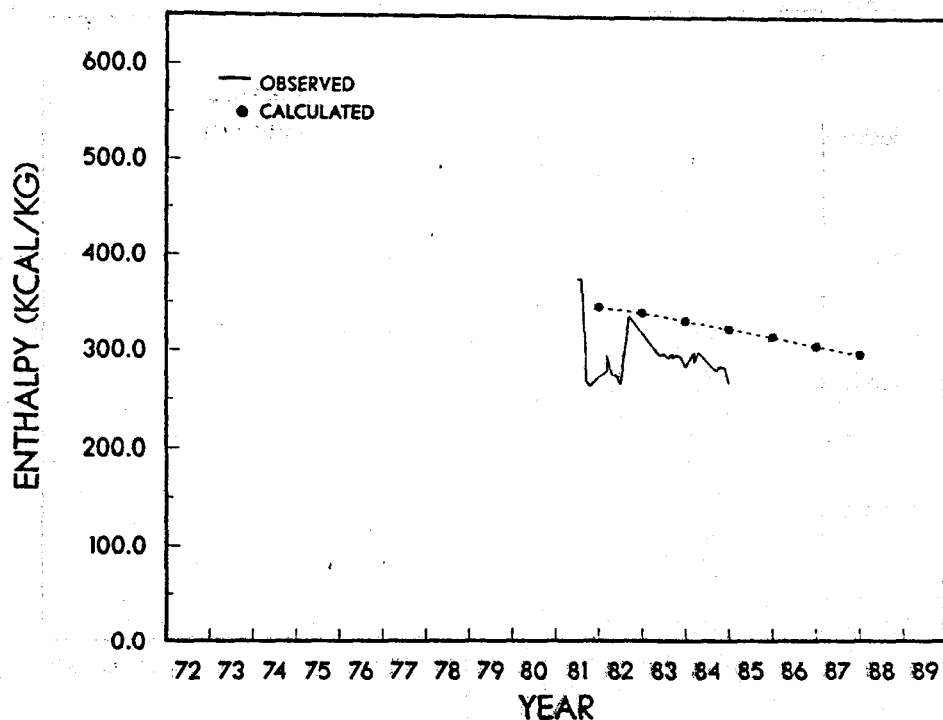


Figure 22. Observed (well E-3) and calculated enthalpy histories for the western upthrown block of the β reservoir, farther to the north of Fault H (near E-3).

Historia de las entalpías observadas (pozo E-3) y calculadas para la zona distante y al norte de la Falla H, en el bloque occidental levantado del yacimiento β (cerca del E-3).

region indicate that there is no boiling and probably cold water recharge is occurring from the north and west.

In the main portion of the western upthrown β reservoir, the calculated enthalpies do not show the observed increasing trend. The model instead presents a slow decrease in enthalpies with time, and some temporary boiling in 1982 (Fig. 21). Except for this early boiling, the observed and calculated enthalpies appear to be approximately the same until around 1984. The increasing values observed after that year could be reproduced by the model by refining the computational mesh and reducing somewhat the permeability assigned to that producing area.

The calculated enthalpies for the northwestern area of this block, north of E-14, are about 50 kcal/kg (about 210 kJ/kg) higher than those observed, and show a decreasing trend as opposed to fairly constant observed values.

Western downthrown block. Pressure data are not available for the western downthrown block of the β reservoir at 2100 m depth. The calculated pressures for this depth (Fig. 23) show a general decreasing trend between 1973 and 1978 (from 188 to about 184 bars), and then the pressure generally declines to 169 bars in 1985, reflecting changes in production rates. The decline in calculated pressures to 158 bars in 1986 is partly due to an increase in production rates in this area of about 30 kg/sec, but is probably mostly because of the significant increase in total fluid extracted from the eastern regions of the β reservoir, associated with the coming on line of CPII and CPIII. This would decrease the inflow of geother-

mal fluids into the western downthrown block of the β reservoir.

The wells completed in this part of the field show fairly constant enthalpies [about 340 kcal/kg (about 1425 kJ/kg); e.g., well M-73, Fig. 24]. No reservoir boiling is occurring in this area, probably because of the cold water recharge from the west and possibly south.

The calculated enthalpies for this region are almost constant. However, they are about 140 kcal/kg (about 585 kJ/kg) lower than the observed ones. The lower calculated enthalpies could result from natural state model temperatures that are too low in the region.

Eastern downthrown block. Figure 24 shows the observed and calculated 1973-1987 pressures for the eastern downthrown block of the β reservoir at 2700 m depth. The observed pressures for the area near well T-366 (data from wells T-366, T-348, T-350, M-119, E-21, E-23, and E-27) show between 1980 and 1987 a decrease from 239 to 188 bars. Based on the available production data, this type of decline was not expected for this portion of the β reservoir. Instead, the pressure was expected to decline in a similar manner as in the eastern upthrown block of the β reservoir, which showed a pressure decrease of about 30 bars in 1986, when the CPII and CPIII power plants came on line. In particular, for the eastern downthrown block of the β reservoir, pre-1986 fluid production was rather insignificant, ranging between 2 and 50 kg/sec (Table 2), which should have only resulted in a general pressure decline of about 10 to 15 bars, at the most. Then, when

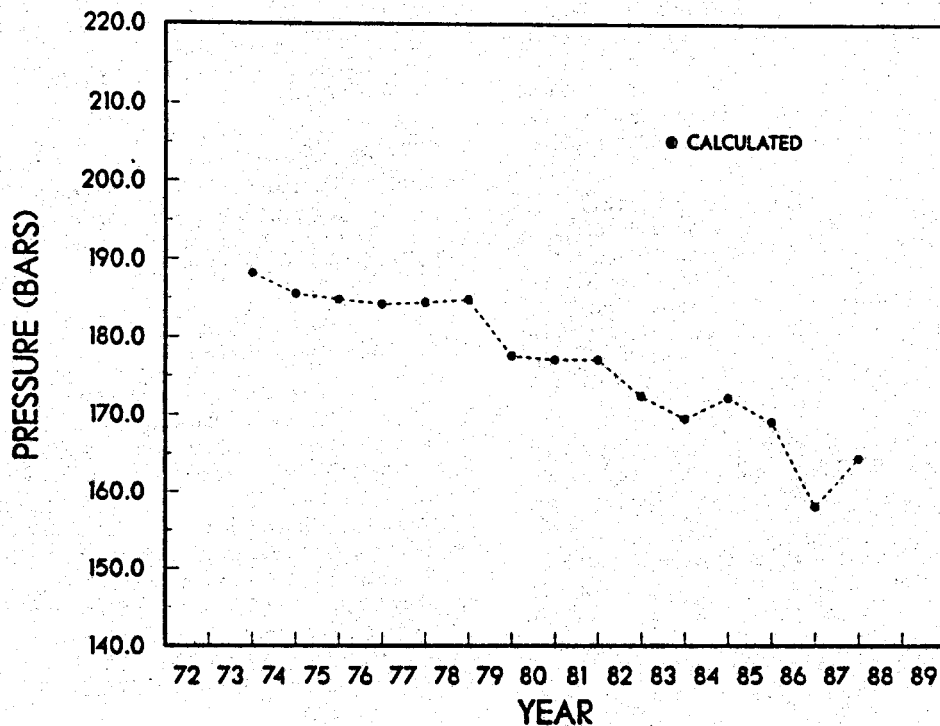


Figure 23. Calculated pressure history for the western downthrown block of the β reservoir.
 Historia de las presiones calculadas para el bloque occidental hundido del yacimiento β .

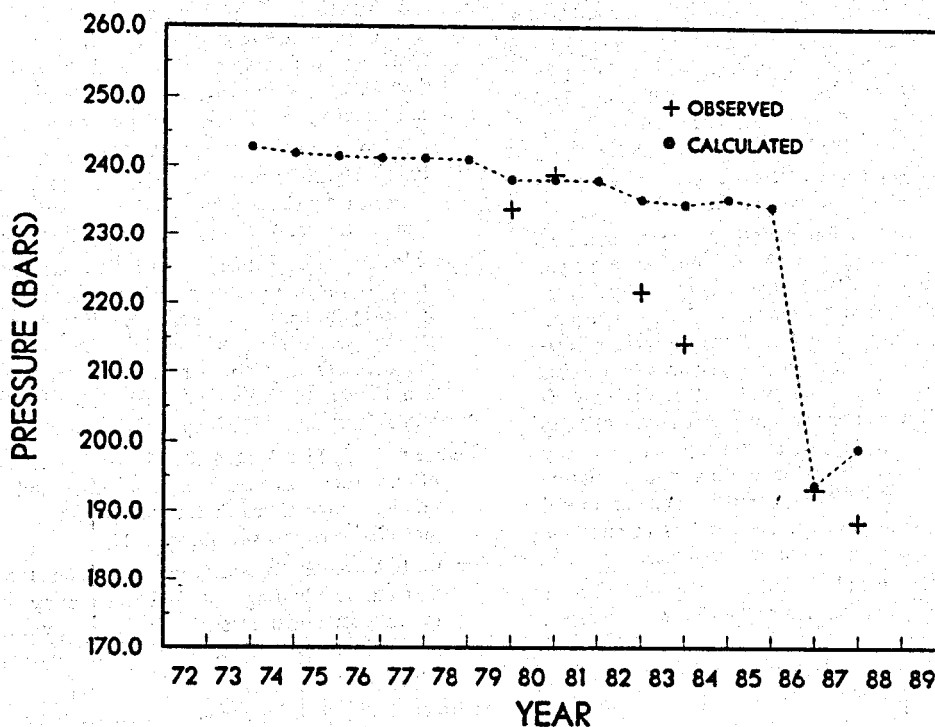


Figure 24. Observed (wells T-366, T-348, T-350, M-119, E-21, E-23, and E-27) and calculated pressure histories for the eastern downthrown block of the β reservoir.
 Historia de las presiones observadas (pozos T-366, T-348, T-350, M-119, E-21, E-23 y E-27) y calculadas para el bloque oriental hundido del yacimiento β .

the production increased from about 2 kg/sec in 1985 to about 940 kg/sec in 1986, a significant drop of at least 30 to 40 bars should have been observed. We cannot explain the observed pressure history shown in Figure 24, unless it is due to significant fluid production of stand-by wells, most of which were "on-bleed", before they were connected to the new power plants. (If this production data becomes available, it will be incorporated into the model.)

As indicated, the calculated and observed pressures for this area do not match (Fig. 24). However, the calculated pressures in the vicinity of T-366 do show a trend that one would have expected based on the production history of Cerro Prieto (Table 2). Between 1973 and 1985 these pressures gradually decline from about 243 to 235 bars. Then, in 1986 a pressure drop of about 35 bars occurred when the new power plants came on line, followed by a small recovery of about 4 bars in 1987.

The 1982-1988 observed enthalpies are fairly constant (340 kcal/kg; about 1425 kJ/kg). The data suggests no reservoir boiling; the area probably has cold water recharge from the east and south.

The calculated enthalpies for this region also tend to be constant, however they are about 180 kcal/kg (about 755 kJ/kg) lower than the observed ones. As in the case of the western upthrown block, in this part of the model the natural state reservoir temperatures in the model seem to be too low.

CONCLUSIONS

After a considerable effort in calibration three-dimensional simulation model of the Cerro Prieto geothermal field has been developed. Even though the computational mesh needs to be refined, it reproduces the basic features of the complex geology of this high-temperature system. For pre-exploitation (natural state) conditions the model gives fluid flow patterns consistent with those of the hydrogeologic model of Halfman et al. (1984, 1986b). There is relative good correspondence between the calculated and observed temperature and pressure distributions throughout the field.

The 1973-1987 exploitation period has been simulated using the geometry and parameters of the natural state model. Fluid production was modeled by incorporating time-dependent sinks in different mesh elements. There is a general good match between observed and computed reservoir pressures and enthalpies. However, some differences still exist that will be reduced by refining the mesh and modifying various parameters in the model, especially permeability (e.g., to change the rate of cold and hot water recharge) and porosity (e.g., to increase/decrease reservoir boiling rates). Future efforts will also include the "tuning" or testing of the model against other type of data, for example changes in reservoir fluid chemistry and surface (or downhole) resistivity.

This study has shown and confirmed the results of other authors i.e., the on-going exploitation of the Cerro Prieto reservoir has resulted in:

- (1) large reservoir pressure drawdown, especially in the eastern regions of the field;
- (2) significant influx of colder waters into the geothermal system along all but its northern boundaries; and
- (3) generalized boiling in the upthrown block of the β reservoir.

There are evidences of localized boiling around wells completed in the α reservoir and some wells in the β reservoir (e.g. Truesdell et al., 1989); this is not reproduced by the model because of the coarseness of the computational mesh.

Even though this is a progress report of an on-going reservoir numerical modeling effort, we tentatively conclude that the reservoir management plan for the Cerro Prieto system needs to be reevaluated to reduce pressure drawdown that results in reservoir boiling, and significant encroachment of colder groundwaters into the system.

ACKNOWLEDGEMENTS

We would like to thank Sally Benson and Karsten Pruess for reviewing the manuscript, and Diana Parks for her assistance in producing the paper. Special thanks are due to our CFE colleagues of the Superintendencia General de Estudios of the Coordinadora Ejecutiva de Cerro Prieto, and of the Departamento de Evaluación y Yacimientos of the Gerencia de Proyectos Geotermoeléctricos for providing the field data used in this study and discussing our results. The work was supported by the Assistant Secretary for Conservation and Renewable Energy, Office of Renewable Energy Technologies, Geothermal Technology Division of the U.S. Department of Energy under contract DE-AC0376SF00098.

REFERENCES

- Bermejo, M., F. J., F. X. Navarro O., F. Castillo B., C.A. Esquer, and C. Cortéz A., 1979. Pressure variations at the Cerro Prieto reservoir during production, Proc. Second Symposium on the Cerro Prieto Geothermal Field, Mexicali, Mexico, Oct. 17-19, 1979, pp. 473-493.
- Elders, W. A., D. K. Bird, A. E. Williams, and P. Schiffman, 1984. Hydrothermal flow regime and magmatic heat source of the Cerro Prieto geothermal system, Baja California, Mexico, *Geothermics*, Vol. 13, pp. 27-47.
- Elders, W. A., A. E. Williams, and J. R. Hoagland, 1981. An integrated model for the natural flow regime in the Cerro Prieto hydrothermal system based upon petrological and isotope geochemical criteria, Proc. Third Symposium on the Cerro Prieto Geothermal Field, March 24-26, 1981, San Francisco, California; Lawrence Berkeley Laboratory Report LBL-11967, pp. 102-109.
- Goldstein, N. E., M. J. Wilt, and D. J. Corrigan, 1984. Analysis of the Nuevo Leon magnetic anomaly and its possible relation to the Cerro Prieto magmatic-hydrothermal system, *Geothermics*, Vol. 13, pp. 3-11.
- Grant, M. A., A. H. Truesdell, and A. Mañón, 1984. Production induced boiling and cold water entry in the Cerro Prieto geothermal reservoir indicated by chemical and physical measurements, *Geothermics*, Vol. 13, pp. 117-140.
- Halfman, S. E., M. J. Lippmann, R. Zelwer, and J. H. Howard, 1984. A geologic interpretation of the geothermal fluid movement in Cerro Prieto field, Baja California, Mexico, *Assoc. Pet. Geol. Bull.*, Vol. 68, pp. 18-30.

- Halfman, S. E., M. J. Lippmann, G. S. Bodvarsson, 1986a. Quantitative model of the Cerro Prieto field, Proc. 11th Workshop on Geothermal Reservoir Engineering, January 21-23, 1986, Stanford, CA, pp. 127-134.
- Halfman, S. E., A. Mañón, and M. J. Lippmann, 1986b. Update of the hydrogeologic model of the Cerro Prieto field based on recent well log data, *Geothermal Resources Council Trans.*, Vol. 10, pp. 369-375.
- León de Vivar, J., 1988. Presencia de dos fases en el yacimiento del campo geotérmico de Cerro Prieto, *Geotermia, Rev. Mex. de Geoenergía*, Vol. 4, No. 1, pp. 203-211.
- Lippmann, M. J., and G. S. Bodvarsson, 1983. Numerical studies of the heat and mass transport in the Cerro Prieto geothermal field, Mexico, *Water Resources Research*, Vol. 19, No. 3, pp. 753-767.
- Lippmann, M. J., A. H. Truesdell, A. Mañón M., and S. E. Halfman, 1989. The hydrogeologic-geochemical model of Cerro Prieto revisited, paper presented at the 14th Workshop on Geothermal Reservoir Engineering, Stanford, CA, January 24-26, 1989.
- Mercado, G. S., 1976. Movement of geothermal fluids and temperature distribution in the Cerro Prieto geothermal field, in Proceedings, Second United Nations Symposium on the Development and Use of Geothermal Resources, May 20-29, 1975, Washington, D.C., U.S., Government Printing Office, Vol. 1, pp. 489-494.
- Pruess, K., 1988. SHAFT, MULKOM AND TOUGH: A set of numerical simulators for multiphase fluid and heat flow, *Geotermia, Rev. Mex. de Geoenergía*, Vol. 4, No. 1, pp. 185-202.
- Rivera, R. J., F. Bermejo, F., Castillo, H. Pérez, and A. Abraján, 1982. Update of the temperature behavior and distribution in Cerro Prieto II and III, Proc. Fourth Symposium on the Cerro Prieto Geothermal Field, Com. Fed. de Elect., Guadalajara, Mexico, August 10-12, 1982, pp. 93-112.
- Truesdell, A. H. and M. J. Lippmann, 1986. The lack of immediate effects from the 1979-1980 Imperial and Victoria earthquakes on the exploited Cerro Prieto geothermal reservoir, *Geothermal Resources Council Trans.*, Vol. 10, pp. 405-411.
- Truesdell, A. H., B. Terrazas, L. Hernández, C. Janik, L. Quijano, and R. Tovar, 1989. The response of the Cerro Prieto reservoir to exploitation as indicated by fluid geochemistry, this volume.